

submitted to *The Astrophysical Journal*

Infrared Emission from Interstellar Dust.

III. The Small Magellanic Cloud

Aigen Li and B.T. Draine

Princeton University Observatory, Peyton Hall, Princeton, NJ 08544, USA;
agli@astro.princeton.edu, draine@astro.princeton.edu

ABSTRACT

The infrared (IR) emission from interstellar dust in the Small Magellanic Cloud (SMC) is modelled using a mixture of amorphous silicate and carbonaceous grains, including a population of polycyclic aromatic hydrocarbon (PAH) molecules. (1) It is shown that this dust model is able to reproduce the spectral energy distribution from near-IR to far-IR for the entire SMC Bar region, provided the PAH abundance in the SMC Bar region is very low. (2) The IR spectrum of the SMC B1#1 molecular cloud can also be reproduced by our dust model provided the PAH abundance is increased relative to the overall SMC Bar. The PAHs in SMC B1#1 incorporate $\sim 3\%$ of the SMC C abundance, compared to $< 0.4\%$ in the SMC Bar. (3) The spectrum of SMC B1#1 is best reproduced if the PAH mixture has intrinsic IR band strengths which differ from the band strengths which best fit Milky Way PAH mixtures. The variation in the PAH IR band strengths would imply different PAH mixtures, presumably a consequence of differing metallicity or environmental conditions. Other possibilities such as superhydrogenation of PAHs and softening of the starlight spectrum are also discussed.

Subject headings: dust, extinction — infrared: ISM: lines and bands — galaxies: individual: SMC

1. Introduction

Due to its low metallicity ($\sim 1/10$ of that in the Milky Way [Dufour 1984]) and low dust-to-gas ratio (over 10 times lower than in the Milky Way [Bouchet et al. 1985]), the Small Magellanic Cloud (SMC) is often considered as a prototype for the interstellar matter in high-redshift galaxies at early stages of chemical enrichment. The analogy is strengthened by the similarities of its typical extinction curve — a nearly linear rise with λ^{-1} (λ is wavelength) and the absence of the 2175Å hump (Lequeux et al. 1982; Prévot et al. 1984; Bouchet et al. 1985; Thompson et al. 1988; Rodrigues et al. 1997; Gordon & Clayton 1998) — to wavelength-dependent extinction inferred for starburst galaxies (Gordon, Calzetti, & Witt 1997) and damped Ly α systems (Pei, Fall, & Bechtold 1991).

Infrared (IR) emission from dust in the SMC has been seen by the *Infrared Astronomical Satellite* (IRAS) (Schwering & Israel 1990; Sauvage, Thuan, & Vigroux 1990), the Diffuse Infrared Background Experiment (DIRBE) instrument on the *Cosmic Background Explorer* (COBE) satellite (Stanimirovic et al. 2000), and the *Infrared Space Observatory* (ISO) (Reach et al. 2000). In the present work we use these observations to test the grain model proposed previously to account for the observed extinction curve for dust in the general SMC Bar region (Weingartner & Draine 2001a).

Of particular interest is the detection by Reach et al. (2000) of the 6.2, 7.7, 8.6, 11.3, and $12.7\mu\text{m}$ emission bands toward the quiescent molecular cloud SMC B1#1. These bands, generally attributed to polycyclic aromatic hydrocarbons (PAHs) (Léger & Puget 1984; Allamandola, Tielens, & Barker 1985), had not previously been observed in the SMC.

The molecular cloud SMC B1#1 ($[\alpha, \delta]_{1950} = [0^{\text{h}}43^{\text{m}}42^{\text{s}}4, -73^{\circ}35'10'']$) has a $11.3\mu\text{m}/7.7\mu\text{m}$ emission band ratio which differs significantly from that for Milky Way regions, such as the ρ Oph reflection nebula (which one might expect SMC B1#1 to resemble [see Reach et al. 2000]); the observed band ratio also falls outside the range which appears to be “allowed” by the PAH model of Li & Draine 2001 (see Figures 16,17 of Draine & Li 2001). The observed spectrum for SMC B1#1 therefore presents an important test which may reveal shortcomings of the current PAH emission models. The unusual band ratio might be indicative of the physical conditions in SMC B1#1, or it might point to systematic differences between the PAH mixtures in the Milky Way and SMC.

In this work we extend the interstellar dust emission model developed for the diffuse interstellar medium (ISM) of the Milky Way (Li & Draine 2001; hereafter LD01) to the SMC, with emphasis on the mid-IR spectrum of SMC B1#1. We seek (1) to test the PAH IR emission model (Draine & Li 2001; LD01); (2) to infer the SMC PAH properties such as size distributions, charging, hydrogenation, and intrinsic IR band strengths; (3) to infer the physical conditions in the SMC and the SMC B1#1 cloud and the dust properties in these environments. Our approach is outlined in §2.1 and §2.2. We first model the spectral energy distribution for the SMC as a whole in §3. Model results for the SMC B1#1 molecular cloud are presented in §4.2–§4.5. In §4.6 we discuss the 2175\AA extinction hump predicted from the present PAH model. Our principal conclusions are summarized in §5.

2. Modelling the Dust IR Emission

2.1. Dust Model

Following LD01, we model the SMC Bar and the SMC B1#1 molecular cloud IR emission as due to a mixture of amorphous silicate grains and carbonaceous grains. We assume that the carbonaceous grain population extends from grains with graphitic properties at radii $a \gtrsim 0.01\mu\text{m}$, down to particles with PAH-like properties at very small sizes.

Dust grains in the SMC and SMC B1#1 are assumed to be heated by a radiation field equal to the Mathis, Mezger, & Panagia (1983; hereafter MMP) estimate of the solar neighbourhood interstellar radiation field (hereafter ISRF),¹ multiplied by a factor U . The IR emissivity per unit solid angle per H nucleon from a mixture of silicate and carbonaceous grains (including both neutral and ionized PAHs) is

$$\begin{aligned} j_\lambda(U) = & \int_{3.5 \text{ \AA}}^{\infty} da \frac{1}{n_{\text{H}}} \frac{dn_{\text{carb}}}{da} \int_0^{\infty} dT B_\lambda(T) \\ & \times \left\{ \phi_{\text{ion}}(U, a) C_{\text{abs}}^{\text{carb}^+}(a, \lambda) \left(\frac{dP^{\text{carb}^+}}{dT} \right) + [1 - \phi_{\text{ion}}(U, a)] C_{\text{abs}}^{\text{carb}^0}(a, \lambda) \left(\frac{dP^{\text{carb}^0}}{dT} \right) \right\} \\ & + \int_{3.5 \text{ \AA}}^{\infty} da \frac{1}{n_{\text{H}}} \frac{dn_{\text{sil}}}{da} \int_0^{\infty} dT B_\lambda(T) C_{\text{abs}}^{\text{sil}} \left(\frac{dP^{\text{sil}}}{dT} \right) \end{aligned} \quad (1)$$

where n_{H} is the hydrogen number density; dn_{carb}/da and dn_{sil}/da are the size distribution functions for carbonaceous and silicate grains, respectively; $C_{\text{abs}}^{\text{carb}^0}$, $C_{\text{abs}}^{\text{carb}^+}$, and $C_{\text{abs}}^{\text{sil}}$ are the absorption cross sections for neutral and ionized carbonaceous grains (including PAHs) and silicate grains, respectively (see LD01); $B_\lambda(T)$ is the Planck function; $dP^{\text{carb}^0}(U, a, T)$, $dP^{\text{carb}^+}(U, a, T)$, and $dP^{\text{sil}}(U, a, T)$ are, respectively, the probabilities that the vibrational temperature will be in $[T, T + dT]$ for neutral and charged PAHs and silicate grains illuminated by starlight intensity U (dP/dT approaches a δ function for large grains); and $\phi_{\text{ion}}(U, a)$ is the probability of finding a PAH molecule of radius a in a non-zero charge state.

For a given radiation intensity U , we calculate the temperature distribution functions dP/dT employing the “thermal-discrete” method which treats both heating (photon absorption) and cooling (photon emission) as discrete transitions, using a thermal approximation for the downward transition probabilities (Draine & Li 2001). We have calculated $P(U, a, T)$ for neutral and ionized PAHs and silicate grains for $0.1 \leq U \leq 10^5$ at intervals of 0.25 in $\log_{10} U$.

Except for single optically-thin clouds, the region observed will generally include material exposed to a range of radiation intensities. We follow Dale et al. (2001) and assume the radiation intensity U to have a power-law distribution of the general form

$$\frac{dN_{\text{H}}}{dU} = \frac{(1 - \beta) N_{\text{H}}^{\text{tot}}}{U_{\text{max}}^{1-\beta} - U_{\text{min}}^{1-\beta}} U^{-\beta}, \quad \text{for } U_{\text{min}} \leq U \leq U_{\text{max}}, \quad \beta \neq 1; \quad (2)$$

$$= \frac{N_{\text{H}}^{\text{tot}}}{\ln(U_{\text{max}}/U_{\text{min}})} U^{-1}, \quad \text{for } U_{\text{min}} \leq U \leq U_{\text{max}}, \quad \beta = 1; \quad (3)$$

where U_{min} and U_{max} are, respectively, the lower and upper cutoff of the radiation intensity U , and $N_{\text{H}}^{\text{tot}}$ is the total hydrogen column density. Lacking knowledge of the detailed geometry of the dust

¹The SMC Bar starlight spectrum may be harder than the MMP ISRF since the SMC has a higher surface density of O and B stars (Lequeux 1989). On the other hand, grains within the SMC B1#1 cloud are exposed to a softer radiation field due to reddening by dust in the cloud (see §4.4). However, in comparison with other uncertainties, these should be considered as second-order effects. We will see in §4.4 that reddening of starlight has only a minor effect on the PAH mid-IR emission band ratios.

and illuminating stars, we will assume the different illumination levels to be randomly distributed along the line-of-sight. The emergent IR intensity is then

$$I_\lambda = \frac{1 - \exp[-N_{\text{H}}^{\text{tot}}\Sigma_{\text{abs}}(\lambda)]}{N_{\text{H}}^{\text{tot}}\Sigma_{\text{abs}}(\lambda)} \int_{U_{\text{min}}}^{U_{\text{max}}} dU \frac{dN_{\text{H}}}{dU} j_\lambda(U) , \quad (4)$$

where $\Sigma_{\text{abs}}(\lambda)$ is the total *absorption*² cross section per H nucleon for the dust model. The integrated IR power per area is $N_{\text{H}}^{\text{tot}}p_0\langle U \rangle$, where p_0 is the absorbed power per H nucleon for dust exposed to starlight with $U = 1$, and the mean starlight intensity $\langle U \rangle$ is

$$\langle U \rangle = \left(\frac{1 - \beta}{2 - \beta} \right) \frac{U_{\text{max}}^{2-\beta} - U_{\text{min}}^{2-\beta}}{U_{\text{max}}^{1-\beta} - U_{\text{min}}^{1-\beta}} , \quad \text{for } \beta \neq 1, 2 ; \quad (5)$$

$$= \frac{U_{\text{max}} - U_{\text{min}}}{\ln(U_{\text{max}}/U_{\text{min}})} , \quad \text{for } \beta = 1 ; \quad (6)$$

$$= \frac{(1 - \beta) \ln(U_{\text{max}}/U_{\text{min}})}{U_{\text{max}}^{1-\beta} - U_{\text{min}}^{1-\beta}} , \quad \text{for } \beta = 2 . \quad (7)$$

2.2. Model Parameters

We have three sets of parameters to be specified or constrained:

1. The column density N_{H} of gas averaged over the beam.
2. The parameters (b_{C} , a_0 , and σ) determining the abundance and size distribution of the “log-normal” population which contributes most of the ultrasmall carbonaceous particles (PAHs).
3. Environmental properties including the starlight intensity U (determined by U_{min} , U_{max} , and β), the electron density n_e , and the gas temperature T_{gas} . The heating and cooling of dust grains are determined by U . The PAH ionization fraction ϕ_{ion} depends on U/n_e , and T_{gas} .

For dust in the general SMC Bar we will adopt the grain size distribution obtained by Weingartner & Draine (2001a) by fitting the extinction curve toward the star AvZ 398 in the SMC Bar (Gordon & Clayton 1998). We will see that the PAHs in the SMC Bar make a negligible contribution to the IR emission. The SMC Bar models therefore depend on just 4 adjustable parameters: U_{min} , U_{max} , β , and $N_{\text{H}}^{\text{tot}}$.

As noted by Reach et al. (2000), SMC B1#1 may be considered to be an analog of the ρ Oph molecular cloud. The dust in the ρ Oph cloud has $R_V \approx 4.2$, so we will assume that the dust grains in SMC B1#1 have the size distribution estimated by Weingartner & Draine (2001a) for Milky Way dust with $R_V = 4.0$ ($b_{\text{C}} = 20$ ppm, Case A), except (1) with abundances relative to H

²If the radiation field in the emitting region is approximately isotropic, scattering does not alter the intensity.

reduced by a factor 10, the SMC gas-to-dust ratio relative to the local Milky Way value (Bouchet et al. 1985), and (2) we allow ourselves the freedom to adjust the parameters b_C , a_0 , and σ .

We adopt a single log-normal size distribution for the PAHs in the SMC B1#1 cloud, characterized by three parameters: a_0 , σ , and b_C ; a_0 and σ respectively determine the peak location and the width of the log-normal distribution, and b_C is the total amount of C atoms relative to H locked up in PAHs. Small PAHs (with $\lesssim 100$ carbon atoms) are expected to be planar (see Appendix A in Draine & Li 2001). The term “PAH radius” used in this and related papers refers to the radius a of a spherical grain with the same carbon density as graphite (2.24 g cm^{-3}) and containing the same number of carbon atoms N_C : $a \equiv 1.288 N_C^{1/3} \text{ \AA}$.

We adopt $n_H \approx 10^3 \text{ cm}^{-3}$, and $T_{\text{gas}} = 15 \text{ K}$ for the SMC B1#1 molecular cloud as estimated by Lequeux et al. (1994) based on observed CO line ratios. After allowance for C in the dust grains, the gas phase C abundance is $[\text{C}/\text{H}]_{\text{gas}} \approx 3 \times 10^{-5}$. In diffuse and translucent regions with $A_V \lesssim 3$, we expect C and other gas-phase metals (Mg, Si, S, Fe) to be photoionized, contributing a fractional ionization $\sim 4 \times 10^{-5}$ in SMC gas. We consider two ionization models: low n_e and high n_e . For the low- n_e model we take $n_e = 0.1 \text{ cm}^{-3}$ ($n_e/n_H \approx 1 \times 10^{-4}$). For the high- n_e model we take $n_e = 1.0 \text{ cm}^{-3}$ ($n_e/n_H \approx 1 \times 10^{-3}$). For the SMC Bar, we take $n_e = 0.1 \text{ cm}^{-3}$. But this is not critical since the amount of PAHs in the SMC Bar is rather small and the PAH mid-IR emission is negligibly low comparing to the far-IR emission (see §3).

For a given n_e , our model for SMC B1#1 is then determined by 7 parameters: U_{min} ; U_{max} ; β ; the dust column $\propto N_H^{\text{tot}}$; the fraction of the dust absorption due to PAHs $\propto b_C$; and the parameters a_0 , σ characterizing the PAH size distribution. We will assume $\sigma = 0.4$ for the width of the PAH size distribution as determined for the diffuse ISM PAHs (LD01). Thus we are left with $N_{\text{par}} = 6$ adjustable parameters: U_{min} , U_{max} , β , N_H^{tot} , b_C , and a_0 .

3. IR Emission from the SMC Bar and Eastern Wing

3.1. Observational Constraints

We first consider the emission from the SMC as a whole. In Figure 1 we plot the surface brightness measured by DIRBE for a 6.25 deg^2 region containing the optical bar and the Eastern Wing (Stanimirovic et al. 2000). The overall spectrum, unlike that of SMC B1#1 (see §4), peaks at $\lambda \sim 100 \mu\text{m}$ with a local minimum at $\lambda \sim 12 \mu\text{m}$.

Stanimirovic et al. (1999) have mapped the HI 21cm emission from the SMC. The total HI mass, corrected for self-absorption, is $\approx 4.2 \times 10^8 M_\odot$ (Stanimirovic et al. 2000). The 6.25 deg^2 region considered here contains $\approx 2.9 \times 10^8 M_\odot$ of HI (S. Stanimirovic 2001, private communication), corresponding to a mean HI column density $\langle N_{\text{HI}} \rangle_{\text{obs}} \approx 5.5 \times 10^{21} \text{ cm}^{-2}$, consistent with $\langle N_{\text{HI}} \rangle \approx 5.0 \times 10^{21} \text{ cm}^{-2}$ determined by Lyman α observations of 21 sightlines (Bouchet et al. 1985). Based on a FUSE (*Far Ultraviolet Spectroscopic Explorer*) survey of H₂ along 26 lines of sight, Tumlinson

et al. (2002) found the H_2/HI mass ratio $M(\text{H}_2)/M(\text{HI}) \lesssim 0.5\%$. However, Israel (1997) suggest a global ratio $M(\text{H}_2)/M(\text{HI}) \approx 20\%$. We take $\langle N_{\text{H}} \rangle_{\text{obs}} \pm \sigma_{\text{H}} = (5.5 \pm 0.5) \times 10^{21} \text{ cm}^{-2}$ for the region considered here.

For a model with N_{par} adjustable parameters, the goodness of fit is measured by

$$\frac{\chi^2}{\text{d.o.f.}} = \frac{([N_{\text{H}}]_{\text{mod}} - \langle N_{\text{H}} \rangle_{\text{obs}})^2 / \sigma_{\text{H}}^2 + \sum_{i=1}^6 ([\lambda I_{\lambda}]_{\text{mod}} - [\lambda I_{\lambda}]_{\text{obs}})^2 / \sigma_i^2}{N_{\text{par}} + 7} \quad (8)$$

measuring the difference between model and observations for the 6.25 deg^2 field studied by Stanimirovic et al. (2000). We use observed 12, 25, 60, 100, 140, and $240\mu\text{m}$ DIRBE band surface brightnesses $[I_{\lambda}]_{\text{obs}}$ and uncertainties σ_i from Stanimirovic et al. (2000).

3.2. Model Results

Grains over such a wide area will be illuminated by a range of radiation fields. We model the SMC DIRBE spectrum assuming a power law distribution for the illuminating radiation (see eq. [2]), using the HI column density $\langle N_{\text{H}} \rangle_{\text{obs}}$ as an additional constraint. As discussed in §2.2, we are left with $N_{\text{par}} = 4$ adjustable parameters: U_{min} , U_{max} , β , and $N_{\text{H}}^{\text{tot}}$.

Our best-fit model (see Table 1) provides a good fit to the entire spectrum with emission from a mixture of silicate and carbonaceous grains with $N_{\text{H}}^{\text{tot}} \approx 5.4 \times 10^{21} \text{ cm}^{-2}$, illuminated by starlight with $U_{\text{min}} = 10^{-1.0}$, $U_{\text{max}} = 10^{2.75}$, $\beta = 1.8$ (see Figure 1a). The small value of $\chi^2/\text{d.o.f.} = 0.2$ suggests that some of the observational uncertainties may have been overestimated.

Our best model has a dust-weighted mean radiation intensity $\langle U \rangle \approx 1.9$. The observed mean surface brightness in the $1.25\mu\text{m}$ DIRBE band averaged over the 6.25 deg^2 field corresponds to only 0.76 of the intensity in the Mathis, Mezger, & Panagia (1983) radiation field, but we expect $\langle U \rangle$ to be larger since the dust is preferentially located in regions of high stellar density.³ Other distributions of radiation intensity are also able to provide a fairly good fit to the observational data, but only if $U_{\text{min}} \lesssim 1$ and $U_{\text{max}} \gtrsim 50$ (see Table 1).

We have also modelled the SMC data using a single U , i.e., assuming that the dust is heated by a uniform radiation field with intensity U . The best-fitting model is given by $U = 10^{1.5}$ and $N_{\text{H}}^{\text{tot}} \approx 2.8 \times 10^{20} \text{ cm}^{-2}$. Although this model provides a fairly good fit to the overall spectrum, the derived hydrogen column density $N_{\text{H}}^{\text{tot}}$ is smaller than measured by a factor of ≈ 20 , giving $\chi^2/\text{d.o.f.} = 10.2$. This model is rejected: the single U model has overestimated the mean radiation field and correspondingly underestimated $N_{\text{H}}^{\text{tot}}$.

³An enhanced radiation field ($\sim 10 - 100$ times the Galactic mean value) is indicated by the observed rotational excitation of H_2 in the SMC diffuse ISM (Tumlinson et al. 2002). This may be due to the fact that the massive stars and H_2 which FUSE observed are located near regions of higher-than-average starlight.

Table 1: Models for SMC Bar and SMC B1#1.

Region	note	n_e^a (cm^{-3})	PAH band strength ^b	a_0 (\AA)	σ	b_C (ppm)	U_{\min} (MMP)	U_{\max} (MMP)	β	$\langle U \rangle$ (MMP)	$N_{\text{H}}^{\text{tot}}$ (10^{21} cm^{-2})	$\chi^2 /$ d.o.f.	A_V^c (mag)	$\Delta A_{2175 \text{ \AA}}$ (mag)
Bar	best	0.01	MW	—	—	0	$10^{-1.0}$	$10^{2.75}$	1.8	1.9	5.4	0.2	0.33	—
Bar	$U_{\min} \uparrow$	0.01	”	—	—	”	$10^{-0.5}$	$10^{2.75}$	2	2.4	4.8	0.9	0.30	—
Bar	$U_{\max} \downarrow$	0.01	”	—	—	”	$10^{-1.0}$	$10^{2.0}$	1.6	2.3	4.8	1.0	0.30	—
Bar	$\beta \downarrow$	0.01	”	—	—	”	$10^{-1.0}$	$10^{1.75}$	1.5	2.4	4.9	1.4	0.30	—
Bar	$\beta \uparrow$	0.01	”	—	—	”	$10^{0.25}$	$10^{3.0}$	2.5	5.1	2.4	5.6	0.15	—
Bar	single U	0.01	”	—	—	”	$10^{1.5}$	$10^{1.5}$	—	32	0.28	10.2	0.02	—
B1#1	best	1.0	SMC	2.8	0.4	1.5	$10^{-0.5}$	$10^{2.5}$	2	2.2	42	1.7	2.05	0.5
B1#1	0.1	MW	3	0.4	1.5	$10^{-0.5}$	$10^{2.5}$	2	2.2	42	5.3	2.05	0.5	
B1#1	1.0	MW	”	”	”	”	”	”	”	”	3.1	”		
B1#1	0.1	Eq.(12)	”	”	”	”	”	”	”	”	3.3	”	”	
B1#1	1.0	Eq.(12)	”	”	”	”	”	”	”	”	1.9	”	”	
B1#1	0.1	SMC	”	”	”	”	”	”	”	”	2.4	”	”	
B1#1	1.0	SMC	”	”	”	”	”	”	”	”	1.8	”	”	
B1#1	0.1	SMC	2.8	0.4	”	”	”	”	”	”	2.1	”	”	

^aElectron density n_e used to calculate the PAH ionization fraction ϕ_{ion} , assuming $T_{\text{gas}} = 15 \text{ K}$.

^b“MW” refers to the PAH band strengths adopted for the Milky Way diffuse ISM (LD01) for which the 6.2, 7.7, and $8.6 \mu\text{m}$ bands have been enhanced (relative to laboratory values) by factors of 3, 2, and 2, respectively; and the H/C ratio is taken as Eq.(11); “Eq.(12)” refers to the same band strengths as those of LD01 but with a higher H/C (see Eq.[12]); “SMC” refers to the laboratory measured band strengths except the $6.2 \mu\text{m}$ band is enhanced by a factor 1.5 (with Eq.[11]).

^cWe adopt $A_V/N_{\text{H}}^{\text{tot}} = 4.9 \times 10^{-23}, 6.2 \times 10^{-23} \text{ mag cm}^2$ respectively for the SMC B1#1 molecular cloud and the SMC Bar (Bouchet et al. 1985; Martin, Maurice, & Lequeux 1989).

3.3. The PAH Abundance in the SMC Bar

The SMC Bar dust model described above consumes $[\text{C}/\text{H}]_{\text{dust}} \approx 15 \text{ ppm}$, and $[\text{Si}/\text{H}]_{\text{dust}} \approx 12 \text{ ppm}$. Our SMC Bar grain model has a very low abundance of PAHs: the $a < 15 \text{\AA}$ carbonaceous grains comprise only $[\text{C}/\text{H}]_{\text{PAH}} \approx 0.2 \text{ ppm}$, consistent with nondetection of the 2175\AA extinction hump (Weingartner & Draine 2001a).

An upper limit on the PAH abundance can be obtained by comparing the DIRBE $12 \mu\text{m}$ and $25 \mu\text{m}$ photometry with theoretical IR spectra calculated for PAH molecules illuminated by the above derived radiation field. We consider PAHs of a single size a . For each size a we obtain an upper limit on $[\text{C}/\text{H}]_{\text{PAH}}$ in PAHs such that this abundance of PAHs would not – by itself – exceed the DIRBE $12 \mu\text{m}$ or $25 \mu\text{m}$ photometry (i.e., we ignore possible additional emission from silicate grains and larger carbonaceous grains). In Figure 2 we show the resulting upper limit $[\text{C}/\text{H}]_{\text{PAH}}$ as a function of PAH size a . It is seen that the DIRBE $25 \mu\text{m}$ band places a stronger constraint than the $12 \mu\text{m}$ band for PAHs $\gtrsim 19 \text{\AA}$; whereas for smaller PAHs ($\lesssim 19 \text{\AA}$) the $12 \mu\text{m}$ photometry provides a stronger constraint. Figure 2 also indicates that $a \approx 12 \text{\AA}$ grains are the best $12 \mu\text{m}$ emitter: the upper limits $[\text{C}/\text{H}]_{\text{PAH}}$ increase as grains either increase or decrease their sizes. In summary, we conclude that the DIRBE $12 \mu\text{m}$ and $25 \mu\text{m}$ photometry places an upper limit of $[\text{C}/\text{H}]_{\text{PAH}} \lesssim 2 \text{ ppm}$ on the abundances of PAHs ($a < 15 \text{\AA}$). This upper bound is much less stringent than the upper limit $[\text{C}/\text{H}]_{\text{PAH}} \lesssim 0.2 \text{ ppm}$ implied by the absence of the 2175\AA extinction hump toward AvZ398.

The paucity of PAH molecules in the SMC Bar, together with the fact that the average

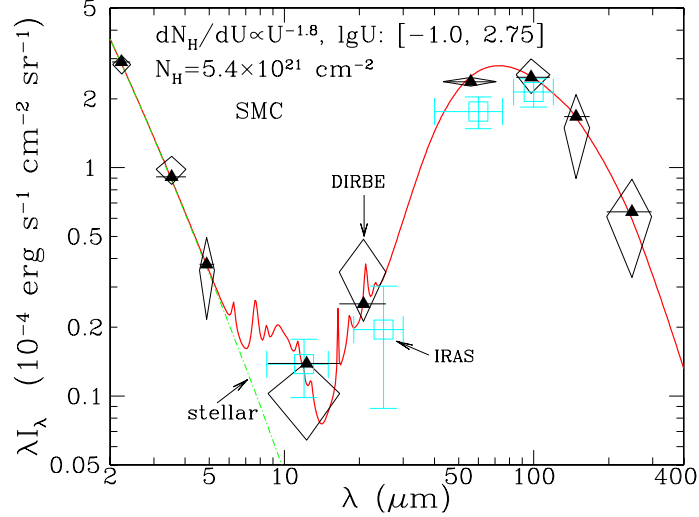


Fig. 1.— Comparison of the model (solid line) to the observed emission from the SMC obtained by COBE/DIRBE (diamonds) and IRAS (squares) averaged over a 6.25 deg^2 region including the optical bar and the Eastern Wing (Stanimirovic et al. 2000). Triangles show the model spectrum convolved with the DIRBE filters. Stellar radiation (dot-dashed line) dominates for $\lambda \lesssim 6\mu\text{m}$. Grains are illuminated by a range of radiation intensities $dN_{\text{H}}/dU \propto U^{-1.8}$, $10^{-1.0} \leq U \leq 10^{2.75}$, with $N_{\text{H}}^{\text{tot}} \approx 5.4 \times 10^{21} \text{ cm}^{-2}$.

extinction curve of the SMC has no observable 2175\AA hump, is consistent with the hypothesis that PAHs are the carriers of the 2175\AA feature. SIRTF 5 – $25\mu\text{m}$ observations of SMC regions where the 2175\AA feature is either very weak or absent could strongly test our dust model, which predicts minimal 7.7 and $11.3\mu\text{m}$ emission features from such regions (as in Figure 1).

4. IR Emission from the SMC B1#1 Cloud

Having seen that our dust model is able to closely reproduce the emission from the SMC as a whole, we now consider the emission from the SMC B1#1 quiescent molecular cloud.

4.1. Observational Constraints

The goodness of fit for SMC B1#1 is measured by

$$\frac{\chi^2}{\text{d.o.f.}} = \frac{\sum_{i=1}^{156} W_i ([\lambda I_{\lambda}]_{\text{mod}} - [\lambda I_{\lambda}]_{\text{obs}})^2 / \sigma_i^2}{N_{\text{par}} + \sum_{i=1}^{156} W_i} \quad (9)$$

where N_{par} is the number of adjustable parameters, $[\lambda I_{\lambda}]_{\text{mod}}$ is the model spectrum (see Eqs.[1,4]), and $[\lambda I_{\lambda}]_{\text{obs}}$ is the observed spectrum.

We use the 5 – $15\mu\text{m}$ ISOCAM spectrum (Reach et al. 2000). For the 150 wavelengths in the

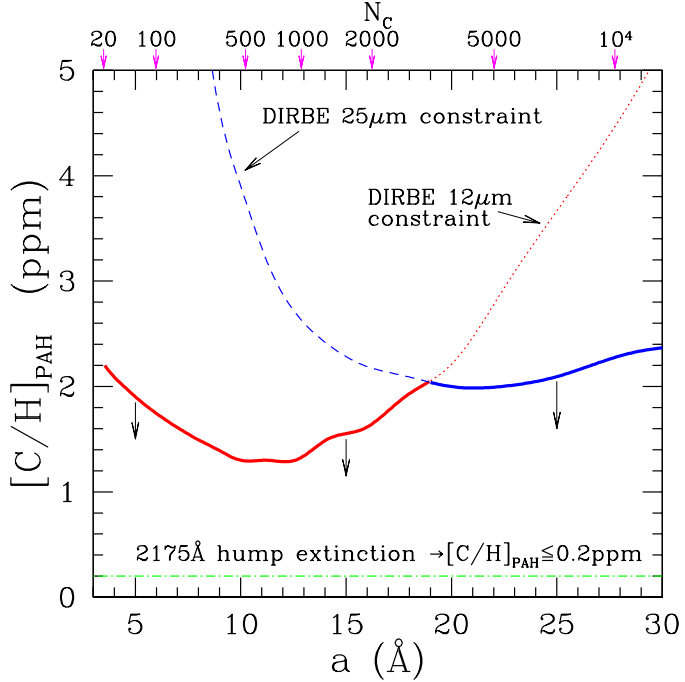


Fig. 2.— Upper limits (solid line) on the abundances of PAHs in the SMC Bar placed by the DIRBE 12 μm and 25 μm band photometry and the 2175 \AA hump extinction (dot-dashed line). Overall, the DIRBE photometry limits the amount of PAHs in the SMC Bar to be $[\text{C}/\text{H}]_{\text{PAH}} \lesssim 2 \text{ ppm}$ (heavy solid line). The absence of the 2175 \AA extinction hump provides the strongest constraint: $[\text{C}/\text{H}]_{\text{PAH}} \lesssim 0.2 \text{ ppm}$ (Weingartner & Draine 2001a). The upper axis indicates the number of C atoms N_{C} in a PAH molecule.

ISO spectrum, the weights W_i are taken to be

$$W_i = \begin{cases} 1, & \text{for } |\lambda - \lambda_{\alpha}| < \gamma_{\alpha}\lambda_{\alpha} \quad (\alpha = 1, 2, \dots, 5); \\ 1/3, & \text{for } |\lambda - \lambda_{\alpha}| > \gamma_{\alpha}\lambda_{\alpha} \quad (\alpha = 1, 2, \dots, 5); \\ 1/6, & \text{for } \lambda < 6.02\mu\text{m} \text{ or } \lambda > 13.38\mu\text{m}; \end{cases} \quad (10)$$

where λ_{α} and $\gamma_{\alpha}\lambda_{\alpha}$ are the peak wavelength and FWHM of the α -th PAH feature (see Table 2), and σ_i is the 1- σ uncertainty in $[\lambda I_{\lambda}]_{\text{obs}}$ at wavelength λ_i .

In addition, we use the IRAS 12, 25, 60, and 100 μm intensities, with $\sigma_i = 0.1(\lambda I_{\lambda})_{\text{obs}}$ (Schwering & Israel 1990); and the DIRBE 140 and 240 μm photometry (Hauser et al. 1998; Schlegel, Finkbeiner, & Davis 1998) after an empirical factor of 1.6 correction for beam dilution⁴, with $\sigma_i = 0.2(\lambda/I_{\lambda})_i$. We assign $W_i = 1$ for the 4 IRAS and 2 DIRBE bands, giving $\sum W_{i=1}^{156} = 93$.

⁴The DIRBE beam size ($0.7^{\circ} \times 0.7^{\circ}$) is much larger than the angular size of the SMC B1#1 cloud ($\sim 50'' \times 40''$, physical size $\sim 10 \text{ pc}$), but there are a number of other emitting clouds in the DIRBE beam. To empirically correct for beam dilution, we multiply the DIRBE 60, 100, 140, and 240 μm surface brightnesses by a factor of 1.6, bringing the DIRBE 60 and 100 μm data into agreement with IRAS (see Figure 4). This provides our best estimate for the emission at 140 and 240 μm .

4.2. Models with Milky-Way PAH Band Strengths

For our initial model, we use IR cross sections $C_{\text{abs}}(a, \lambda)$ for neutral and charged PAHs following LD01. We use the band strengths $\int S_\alpha(\lambda) d\lambda^{-1}$ recommended by LD01 for the Milky Way (MW) PAH mixture where $S_\alpha(\lambda)$ is the absorption cross section per C atom, but we adjust central wavelengths λ_α and FWHMs $\gamma_\alpha \lambda_\alpha$ of the mid-IR features to match the observed spectrum. Table 2 shows the canonical MW band positions and FWHM (from LD01) and the values appropriate for SMC B1#1 (see also Table 1 in Reach et al. 2000). Most of the changes are small, but the 11.3 and $12.7\mu\text{m}$ features in SMC B1#1 are approximately twice as wide as for MW PAH mixtures, while the $7.7\mu\text{m}$ feature is $\sim 25\%$ narrower than in the MW.

Table 2: Drude Profile Parameters for PAHs

α	$\lambda_\alpha(\mu\text{m})^a$		$\gamma_\alpha \lambda_\alpha(\mu\text{m})^b$		E_α^c	
	MW ^d	SMC ^e	MW ^d	SMC ^e	MW ^d	SMC ^f
1	6.20	6.26	0.20	0.24	3	1.5
2	7.70	7.65	0.70	0.53	2	1
3	8.60	8.48	0.40	0.36	2	1
4	11.30	11.34	0.20	0.54	1	1
5	12.70	12.80	0.30	0.58	1	1

^aCentral wavelength.

^bFWHM.

^cEnhancement of band strength $\int S_\alpha(\lambda) d\lambda^{-1}$ relative to average of lab values (see Table 1 of LD01).

^dParameters recommended by LD01 for diffuse regions in the Milky Way.

^eParameters giving good agreement with position and FWHM of 5-15 μm features for the SMC B1#1 molecular cloud (see §4.2).

^fBand strengths giving good agreement with spectrum of the SMC B1#1 molecular cloud (see §4.5).

The PAH absorption cross sections $C_{\text{abs}}(a, \lambda)$ and the temperature probability distribution functions dP/dT depend upon the number of C atoms and the H/C ratio in the molecule. As a starting point, we take H/C to be

$$\text{H/C} = \begin{cases} 0.5, & N_C \leq 25, \\ 0.5/\sqrt{N_C/25}, & 25 \leq N_C \leq 100, \\ 0.25, & N_C \geq 100, \end{cases} \quad (11)$$

which is appropriate for compact, symmetric PAHs for $N_C \lesssim 10^2$, and clusters of such PAHs for $N_C \gtrsim 10^2$. Draine & Li (2001) found that the prescription (11) appears to be consistent with the 3-15 μm emission spectrum seen in reflection nebulae and photodissociation regions in the Milky Way.

For a given n_e and a given radiation intensity U , we estimate the PAH ionization fractions $\phi_{\text{ion}}(U, a)$ in SMC B1#1 using the rates for photoelectric emission and electron capture recently

discussed by Weingartner & Draine (2001b). Figure 3 shows the ionization fractions calculated for a range of radiation intensities and PAH sizes. At low U/n_e , PAHs are more likely to be negatively charged (e.g., $\phi_{\text{ion}^+} < \phi_{\text{ion}^-}$ for $U/n_e \lesssim 10 \text{ cm}^{-3}$; see Figure 3a,b) since the charging of a neutral PAH is dominated by electron capture.

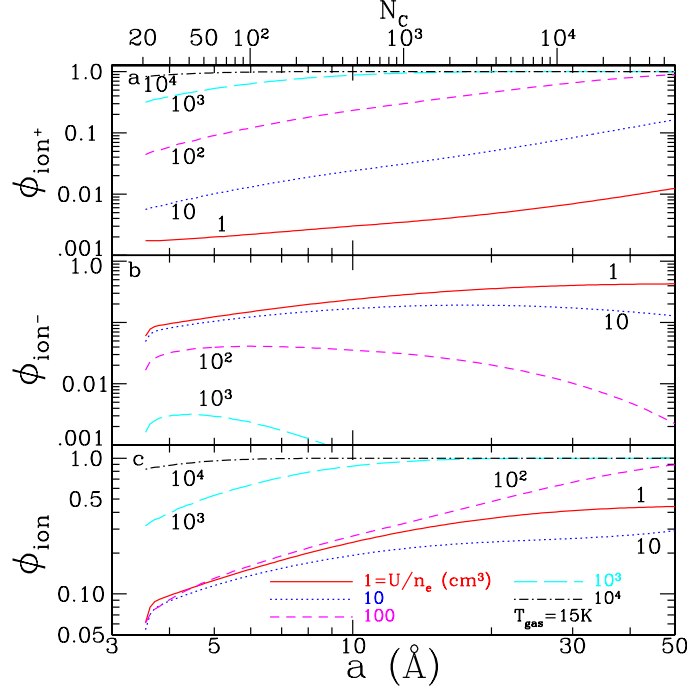


Fig. 3.— The fraction of positively charged (a), negatively charged (b), and non-neutral (c) PAHs as a function of size and radiation intensity for $n_e = 0.1 \text{ cm}^{-3}$ and $T_{\text{gas}} = 15 \text{ K}$. The upper axis label gives the number of carbon atoms $N_C = 0.468(a/\text{\AA})^3$.

For each of our two trial n_e values, we adjust U_{min} , U_{max} , β , a_0 , $N_{\text{H}}^{\text{tot}}$, and b_{C} to minimize χ^2 . In Figure 4a,b we plot the best-fitting model spectrum for our low- n_e model, for which $U_{\text{min}} = 10^{-0.5}$, $U_{\text{max}} = 10^{2.5}$, $\beta = 2$, $a_0 = 3 \text{\AA}$, $\sigma = 0.4$, $b_{\text{C}} = 1.5 \text{ ppm}$, and $N_{\text{H}}^{\text{tot}} \approx 4.2 \times 10^{22} \text{ cm}^{-2}$ (parameters are summarized in Table 1). Our estimate for the mean radiation intensity $\langle U \rangle \approx 2.2$ is consistent with $U \approx 3$ (with an uncertainty of a factor 2) estimated by Reach et al. (2000). We estimate that the dust in SMC B1#1 provides an extinction $A_V \approx 2.1 \text{ mag}$.

Although the model closely reproduces the 12, 25, 60, 100, 140, and 240 μm IRAS/DIRBE photometry (the 2.2, 3.5, and 4.9 μm DIRBE bands are well represented by 6500 K black-body stellar radiation), the model is not fully successful in reproducing the 6–13 μm PAH emission features, resulting in the relatively large $\chi^2/\text{d.o.f.} \approx 5.3$. In particular, it is a bit too weak for the 11.3 μm C-H out-of-plane bending mode while too strong for the 7.7 μm C-C stretching mode.

In view of the fact that the 11.3 μm feature is much stronger in neutral PAHs than in charged PAHs (Allamandola, Hudgins, & Sandford 1999), the 11.3 μm feature deficit could be alleviated by

increasing n_e so as to reduce the PAH ionization fraction (see Figure 3). Indeed, it is seen in Figure 4d that our high n_e model provides an improved fit, with $\chi^2/\text{d.o.f.} \approx 3.1$. The unphysical case of *pure neutral* PAHs leads to a better fit (see Figure 4f; $\chi^2/\text{d.o.f.} \approx 1.9$), but is still deficient in the $11.3\mu\text{m}$ band. We discuss this further in §4.3.

For both low- n_e and high- n_e models, the number of C atoms (relative to H) in PAHs required to account for the SMC B1#1 mid-IR spectrum is $b_C \approx 1.5$ ppm. The total C and Si abundances locked up in dust ($[\text{C}/\text{H}]_{\text{dust}} \approx 24.2$ ppm; $[\text{Si}/\text{H}]_{\text{dust}} \approx 4.1$ ppm) are consistent with the overall SMC elemental abundance ($\text{C}/\text{H} \approx 54$ ppm, $\text{Si}/\text{H} \approx 11$ ppm, $\text{Mg}/\text{H} \approx 9.6$ ppm, $\text{Fe}/\text{H} \approx 6.9$ ppm; Russell & Dopita 1992).

Finally, we remark that models with a single value of U are unable to provide a satisfactory fit to the SMC B1#1 $60\mu\text{m}$ flux unless we add a log-normal PAH component peaking at $\sim 40 - 50\text{\AA}$ containing a substantial mass (e.g. $\text{C}/\text{H} > 8$ ppm for $U = 3$).

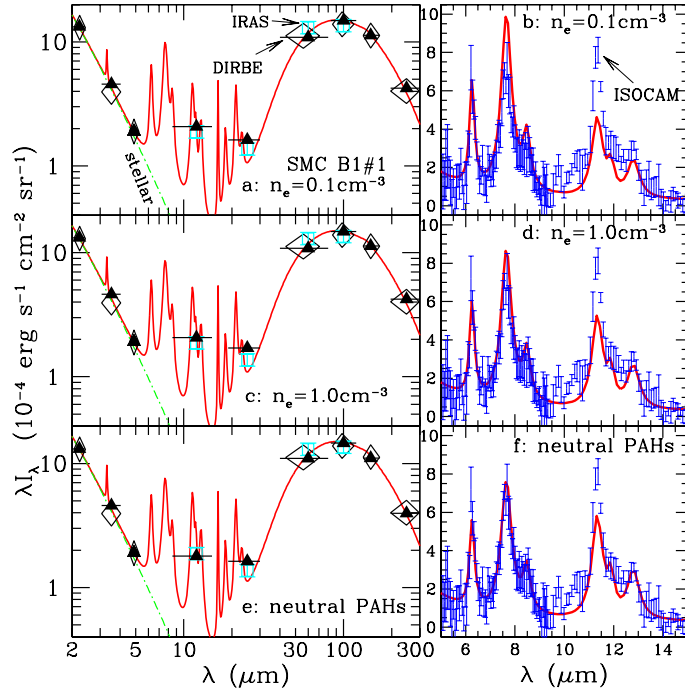


Fig. 4.— Comparison of the model (solid line) to IRAS photometry (squares), DIRBE photometry (diamonds), and 5–15 μm ISOCAM spectroscopy (vertical bars in panels b, d, and f) of the quiescent molecular cloud SMC B1#1. Triangles show the model spectrum convolved with the IRAS (12, 25, 60, 100 μm) and DIRBE (140, 240 μm) filters. Stellar radiation (dot-dashed line) is approximated by a 6500 K black-body. Upper panels (a,b): the best-fit low- n_e dust model ($a_0 = 3\text{\AA}$, $\sigma = 0.4$, $b_C = 1.5$ ppm; $n_e = 0.1\text{ cm}^{-3}$; $\chi^2/\text{d.o.f.} \approx 5.3$) illuminated by a range of radiation intensities $dN_{\text{H}}/dU \propto U^{-2}$, $10^{-0.5} \leq U \leq 10^{2.5}$, with $N_{\text{H}}^{\text{tot}} \approx 4.2 \times 10^{22}\text{ cm}^{-2}$. Middle panels (c,d): same as (a,b) but for the high- n_e model ($n_e = 1.0\text{ cm}^{-3}$; $\chi^2/\text{d.o.f.} \approx 3.1$). Lower panels (e,f): same as (a,b) but for a *pure neutral*-PAH dust model ($\chi^2/\text{d.o.f.} \approx 1.9$).

4.3. Models with Increased PAH Hydrogenation

It is seen in Figure 4 that even when entirely neutral our PAH model is still too weak in the $11.3\mu\text{m}$ band. Reach et al. (2000) suggested that the strong emission in the $11.3\mu\text{m}$ C-H bending mode might be due to increased hydrogenation of the SMC PAHs, which might perhaps be related to the fact that the gas phase C abundance (relative to H) is a factor of 10 lower than in the Milky Way (Dufour 1984; Russell & Dopita 1992). To test this hypothesis, we have considered a PAH model where we assume the same intrinsic band strengths for C-C and C-H stretching and bending modes, but with a higher H/C ratio (which would be appropriate for PAHs with more open structures):

$$\text{H/C} = \begin{cases} 0.5, & N_{\text{C}} \leq 100, \\ 0.5/\sqrt{N_{\text{C}}/100}, & 100 \leq N_{\text{C}} \leq 400, \\ 0.25, & N_{\text{C}} \geq 400. \end{cases} \quad (12)$$

We find that the best-fitting spectra (see Figure 5) do lead to improvements over those calculated from PAHs with a lower degree of hydrogenation (see Eq.[11]).

However, this high H/C model still fails to attain the observed $11.3\mu\text{m}/7.7\mu\text{m}$ band ratio even taking all PAHs to be neutral (see Figure 5c). An increase in a_0 and/or σ (implying a larger ϕ_{ion} [see Figure 3] and a smaller H/C [see Eq.12]) does not help since this would lead to a decrease at the $11.3\mu\text{m}$ band. While a slight decrease in a_0 and/or σ (implying a smaller ϕ_{ion} [see Figure 3] and a higher H/C [see Eq.12]) would result in an increase at the $11.3\mu\text{m}$ band, this results in a decrease at the 6.2 , and $7.7\mu\text{m}$ bands and thus does not work either since this model is already deficient in the 6.2 and $7.7\mu\text{m}$ bands (see Figure 5f).

In comparison with normal PAHs, super-hydrogenated PAHs would produce a stronger $3.3\mu\text{m}$ C-H stretching feature, a broad plateau below the 3.4 and $3.5\mu\text{m}$ features (Bernstein, Sandford, & Allamandola 1996; Pauzat & Ellinger 2001), and a stronger $6.2\mu\text{m}$ C-C stretching feature (Beegle, Wdowiak, & Harrison 2001). Future high-resolution observations of SMC B1#1 particularly at the $3\mu\text{m}$ region, will provide us with more information about the PAH hydrogenation.

Since Milky Way PAHs with $\gtrsim 25$ C atoms are expected to be already essentially fully hydrogenated (Tielens et al. 1987; Allamandola, Tielens, & Barker 1989; Allain, Leach, & Sedlmayr 1996), an increase in the H/C ratio in the SMC would require that the PAHs have more open structures than in the Milky Way. There is no apparent reason to expect this difference in PAH structure between the Milky Way and SMC. Based on an analysis of the $10\text{--}15\mu\text{m}$ PAH out-of-plane C-H bending features, Vermeij et al. (2002) argue that the PAH emission in the SMC B1#1 cloud is dominated by compact PAHs, i.e., relatively low hydrogenation. In conclusion, it appears unlikely that the large $11.3\mu\text{m}/7.7\mu\text{m}$ band ratio in SMC B1#1 is attributable to enhanced hydrogenation.

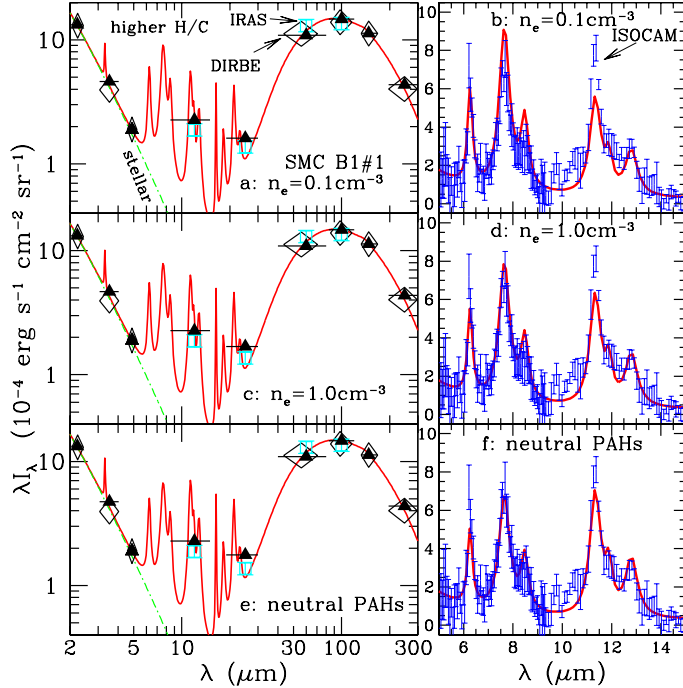


Fig. 5.— Same as Figure 4 but for PAHs with a higher degree of hydrogenation (see Eq.[12]).

4.4. Reddened Starlight?

In previous sections the interstellar radiation field is taken to have the same spectrum as the MMP solar neighbourhood field. Although this assumption seems reasonable for the overall SMC where the extinction is small ($A_V \approx 0.3$ mag; see §3), the starlight incident on the SMC B1#1 molecular cloud surface will be subject to considerable reddening inside the cloud ($A_V \approx 2$ mag; see §4). The reddened starlight will affect the PAH emission bands in two ways: (1) PAH molecules will be excited to lower temperatures; (2) the probability of being (positively) charged (via photoelectron ejection) will be smaller. One therefore would expect an increase in the $11.3\mu\text{m}/7.7\mu\text{m}$ band ratio. Could reddening of the starlight explain the observed $11.3\mu\text{m}/7.7\mu\text{m}$ band ratio in SMC B1#1?

To investigate this, we consider a trial reddened radiation field with the spectrum shown in Figure 6a, with a factor of ~ 3 reduction in the relative intensity at $0.1\mu\text{m}$ relative to $0.5\mu\text{m}$. We have calculated the temperature probability distribution functions for PAHs excited by this radiation field with $U = 1$. The mid-IR emission spectrum is entirely due to single-photon heating, so the emission per PAH simply scales as U ; the spectrum in the lower panel of Figure 6 is calculated for $U = 2.2$. It is seen in Figure 6b that even for pure neutral PAHs, reddened starlight results in an emission spectrum which is very similar to the pure neutral PAH spectrum in the unreddened radiation field in Figure 4f, and is unable to reproduce the observed $11.3\mu\text{m}/7.7\mu\text{m}$ band ratio. We conclude that excitation by reddened starlight cannot account for the $11.3\mu\text{m}/7.7\mu\text{m}$ band ratio observed toward SMC B1#1.

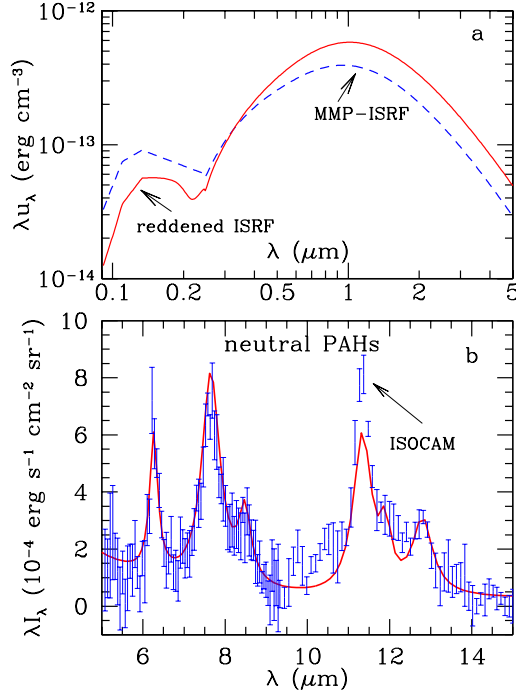


Fig. 6.— Upper panel (a): trial reddened ISRF spectrum (solid line) with energy density equal to the MMP ISRF ($U = 1$). Also plotted is the MMP ISRF ($U = 1$; dashed line). Lower panel (b): the best-fit pure neutral-PAH model ($a_0 = 2.6 \text{ \AA}$, $\sigma = 0.4$, $b_C = 1.5 \text{ ppm}$, and $N_H \approx 4.5 \times 10^{22} \text{ cm}^{-2}$ [for $\langle U \rangle \approx 2.2$; $\chi^2/\text{d.o.f.} \approx 1.9$]).

4.5. IR Band Strengths: Milky-Way PAHs vs. SMC PAHs

Individual PAHs differ considerably in the relative strengths of different vibration bands. LD01 discussed laboratory measurements and theoretical calculations of band strengths for selected PAH molecules and ions, but argued that spectroscopy of various objects in the Milky Way was best reproduced if the 6.2, 7.7 and $8.6 \mu\text{m}$ band strengths were increased by factors of $E_{6.2} = 3$, $E_{7.7} = 2$, and $E_{8.6} = 2$ respectively, relative to the average laboratory and theoretical values. These enhancement factors were used for the models shown in Figures 4–6.

It is reasonable to ask whether the observed spectrum indicates that the band strengths for the PAHs in SMC B1#1 differ from the band strengths which characterize PAHs in the Milky Way. If so, what band strengths give the best fit to the SMC B1#1 spectrum?

In Figure 7 we show the emission calculated from a model with $E_{6.2} = 1.5$, $E_{7.7} = E_{8.6} = 1$. For $n_e = 1.0 \text{ cm}^{-3}$ this model (see parameters in Table 1) is in very good agreement with the observations, with $\chi^2/\text{d.o.f.} = 1.7$. The agreement is considerably better than for the models considered in Figures 4–6. Note that these adjusted band strengths are in fact *closer* to the average laboratory values than are the “Milky Way” band strengths.

Alternatively, the apparent need for a change in intrinsic band strength might be due to the

oversimplification of the “astronomical” PAH model in which we do not distinguish anions (PAH^-) and multiply-charged cations (PAH^{n+}) from singly-charged cations (PAH^+). Bauschlicher & Bakes (2000) predict that the $6.2, 7.7\mu\text{m}$ C-C stretching modes and the $8.6\mu\text{m}$ in-plane C-H bending mode are even more enhanced for PAH^{n+} than PAH^+ . PAH^- anions have band strengths intermediate between those of neutrals (strong $3.3\mu\text{m}$ C-H stretching and $11.3, 11.9, 12.7\mu\text{m}$ out-of-plane C-H bending modes) and PAH^+ cations (strong $6.2, 7.7\mu\text{m}$ C-C stretching and $8.6\mu\text{m}$ C-H in-plane bending mode). Unfortunately, no experimental measurements have yet been made for multiply-ionized PAHs. Available evidence indicates that the IR properties of PAH^- anions closely resemble those of PAH^+ cations except for the very strong $3.3\mu\text{m}$ C-H stretch enhancement in the anion (Szczepanski, Wehlburg, & Vala 1995; Hudgins et al. 2000).

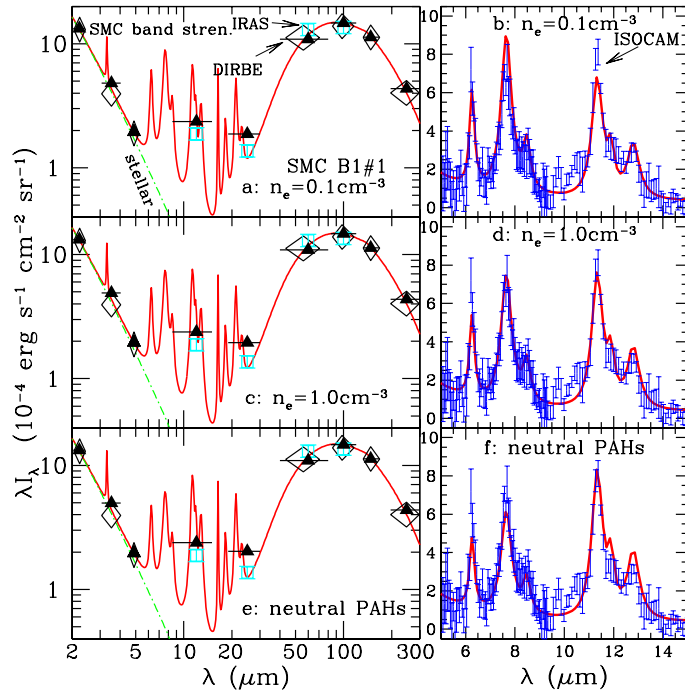


Fig. 7.— Same as Figure 4 but for PAHs with “SMC” band strengths (see text) and a size distribution of $a_0=2.8\text{\AA}$ and $\sigma=0.4$. We favor this model with $n_e \approx 1.0\text{ cm}^{-3}$ for SMC B1#1.

4.6. UV Extinction

Laboratory measurements show that PAHs have an absorption peak due to the $\pi-\pi^*$ electronic transition in the vicinity of $2000-2500\text{\AA}$, and in the grain model considered here (LD01) it is assumed that the interstellar PAH mixture contributes absorption with the wavelength-dependence of the 2175\AA feature observed on sightlines in the Milky Way and the Large Magellanic Cloud (LMC). The PAH abundance required to reproduce the observed IR emission features in the Milky Way ($\text{C/H} \approx 60\text{ ppm}$) is such that we posit that PAHs in fact contribute most of the observed 2175\AA

feature. The predicted extinction excess at 2175Å is (see LD01)

$$\Delta A_{2175\text{\AA}} \approx 0.85 (b_{\text{C}} N_{\text{H}} / 10^{17} \text{ C cm}^{-2}) \text{ mag} . \quad (13)$$

Our best-fitting model has $N_{\text{H}} = 4.2 \times 10^{22} \text{ cm}^{-2}$ and $b_{\text{C}} = 1.5 \text{ ppm}$ (see §4). Therefore we predict $\Delta A_{2175\text{\AA}} \approx 0.5 \text{ mag}$ for sightlines through SMC B1#1. We note that the $\Delta A_{2175\text{\AA}}$ value derived here is a lower limit since $15 \lesssim a \lesssim 150 \text{ \AA}$ carbonaceous grains may also contribute to the 2175Å hump.

This prediction appears to conflict with the fact that most SMC extinction curves have no detectable 2175Å hump (Prévet et al. 1984). However, as pointed out by Reach et al. (2000), there may be regional variations in the SMC extinction curve. We note that the sight lines which show no 2175Å hump all pass through the SMC Bar regions of active star formation (Prévet et al. 1984; Rodrigues et al. 1997; Gordon & Clayton 1998). There is at least one line of sight (Sk 143=AvZ 456) with an extinction curve with a strong 2175Å hump (Lequeux et al. 1982; Prévet et al. 1984; Bouchet et al. 1985; Thompson et al. 1988; Rodrigues et al. 1997; Gordon & Clayton 1998). This sightline passes through the SMC wing, a region with much weaker star formation (Gordon & Clayton 1998). It is possible that the SMC B1#1 dust, just like the dust toward Sk 143, has been exposed to a less harsh environment than that in the SMC Bar regions where the UV extinction has been measured, and where the radiation and shocks associated with massive stars might have destroyed PAHs. Finally, we also note that *both* the 2175Å hump (Fitzpatrick 1985) *and* PAH emission features (Sturm et al. 2000) are present in the 30 Dor region in the LMC, another low-metallicity environment ($\sim 1/4$ of that in the Milky Way; Dufour 1984).

5. Conclusions

In contrast to the Milky Way Galaxy, the SMC is characterized by a lower metallicity, a lower dust-to-gas ratio, and an absence of the 2175Å hump on most sightlines with measured UV extinction (see §1). Therefore, the SMC provides an ideal laboratory to study dust in an environment quite different from the Milky Way. We have modelled the IR spectral energy distribution for the SMC as a whole (averaged over a 6.25 deg^2 area) (§3). We have also modelled the IR emission spectrum of the quiescent molecular cloud SMC B1#1 (§4). Our principal results are:

1. The dust IR emission from a 6.25 deg^2 region including the SMC Bar and Eastern Wing is well reproduced by a model with $dN_{\text{H}}/dU \propto U^{-1.8}$, $10^{-1.0} \leq U \leq 10^{2.75}$, and $N_{\text{H}}^{\text{tot}} \approx 5.4 \times 10^{21} \text{ cm}^{-2}$ using the SMC dust model of Weingartner & Draine (2001a). This dust has a very low PAH abundance, with C/H $\lesssim 0.2 \text{ ppm}$ ($\lesssim 0.4\%$ of the SMC interstellar C abundance) incorporated into PAHs. The dust-weighted mean radiation intensity is $\langle U \rangle \approx 2$, but the starlight intensity must have a broad distribution ranging from $U_{\text{min}} \lesssim 0.3$ to $U_{\text{max}} \gtrsim 50$ (§3).
2. The IR emission from the molecular cloud SMC B1#1 can be reproduced by a dust model consisting of silicates, graphite, and PAHs with $N_{\text{H}}^{\text{tot}} \approx 4.2 \times 10^{22} \text{ cm}^{-2}$ illuminated by starlight

with a power law distribution $dN_{\text{H}}/dU \propto U^{-2}$, $10^{-0.5} \leq U \leq 10^{2.5}$ (§4). The required PAH abundance in SMC B1#1 is 1.5 ppm, or $\sim 3\%$ of the SMC interstellar C abundance.

3. The observed $11.3\mu\text{m}/7.7\mu\text{m}$ and $6.2\mu\text{m}/7.7\mu\text{m}$ band ratios for SMC B1#1 fall outside the “allowed” region predicted for the Milky Way PAH model (see Figures 16, 17 of Draine & Li 2001). In §4.2, §4.3, and §4.4, we examine the possibility that this could be due to (1) an enhanced neutral fraction, (2) an enhanced H/C ratio for the PAHs in SMC B1#1, or (3) reddening of the radiation field to which the PAHs in SMC B1#1 are exposed, but none of these scenarios successfully accounts for the observed $5\text{--}15\mu\text{m}$ spectrum. We instead conclude that the intrinsic IR band strengths for the PAH mixture in SMC B1#1 differ from the band strengths adopted for Milky Way PAH mixtures (§4.5). This indicates that the PAH mixture in SMC B1#1 differs in detail from the PAH mixtures present in a number of Milky Way regions. The band strengths suggested by the SMC B1#1 spectrum are close to “laboratory” band strengths.
4. The PAH abundance in SMC B1#1 exceeds that in the SMC Bar by a factor $\gtrsim 8$ (C/H=1.5 ppm vs $\lesssim 0.2\text{ppm}$). While the average SMC extinction curve has no detectable 2175\AA hump, we predict a 2175\AA extinction excess of $\gtrsim 0.5\text{ mag}$ for the dust in SMC B1#1 (§4.6).

Two types of measurements would be of great value to test our dust model: (1) UV extinction measurements for sightlines through or near SMC B1#1 to test for the predicted 2175\AA feature; (2) $3\text{--}15\mu\text{m}$ spectrophotometry of other regions in the SMC where UV extinction measurements place a strong upper limit on the 2175\AA feature – the present model predicts that PAH emission should not be seen from such regions.

We thank W.T. Reach for providing us with the ISO spectrum of SMC and for helpful comments; D.P. Finkbeiner for help in obtaining the DIRBE fluxes for the SMC B1#1 molecular cloud; S. Stanimirovic for obtaining the SMC HI mass; G. Helou for valuable comments; and R.H. Lupton for the availability of the SM plotting package. This research was supported in part by NASA grant NAG5-10811 and NSF grant AST-9988126.

REFERENCES

Allain, T., Leach, S., & Sedlmayr, E. 1996, A&A, 305, 602

Allamandola, L.J., Tielens, A.G.G.M., & Barker, J.R. 1985, ApJ, 290, L25

Allamandola, L.J., Tielens, A.G.G.M., & Barker, J.R. 1989, ApJS, 71, 733

Allamandola, L.J., Hudgins, D.M., & Sandford, S.A. 1999, ApJ, 511, L115

Bauschlicher, C., & Bakes, E.L.O. 2000, Chem. Phys., 262, 285

Beegle, L.W., Wdowiak, T.J., & Harrison, J.G. 2001, Spectrochim Acta A 57, 737

Bernstein, M.P., Sandford, S.A., & Allamandola, L.J. 1996, ApJ, 472, L127

Bouchet, P., Lequeux, J., Maurice, E., Prévot, L., & Prévot-Burnichon, M. L. 1985, A&A, 149, 330

Dale, D.A., Helou, G., Contursi, A., Silbermann, N.A., & Kolhatkar, S. 2001, ApJ, 549, 215

Draine, B.T., & Li, A. 2001, ApJ, 551, 807

Dufour, R.J. 1984, in IAU Symp. 108, Structure and Evolution of the Magellanic Clouds, ed. S. van den Bergh, & K.S. de Boer (Dordrecht: Reidel), 353

Fitzpatrick, E.L. 1985, ApJ, 299, 219

Gordon, K.D., & Clayton, G.C. 1998, ApJ, 500, 816

Gordon, K.D., Calzetti, D., & Witt, A.N. 1997, ApJ, 487, 625

Hauser, M.G., Kelsall, T., Leisawitz, D., & Weiland, J. 1998, COBE Diffuse Infrared Background Experiment Explanatory Supplement version 2.3, COBE Ref. Pub. No. 98-A (Greenbelt, MD: NASA GSFC), available in electronic form from the NSSDC

Hudgins, D.M., Bauschlicher, C.W., Allamandola, L.J., & Fetzer, J.C. 2000, J. Phys. Chem., 104, 3655

Israel, F.P. 1997, A&A, 328, 471

Léger, A., & Puget, J.L. 1984, A&A, 137, L5

Lequeux, J. 1989, in Recent Developments of Magellanic Cloud Research, ed. K.S. de Boer, G. Stasinska, & Spite, F. (Observatoire de Paris: Paris), 119

Lequeux, J., Maurice, E., Prévot-Burnichon, M.-L., Prévot, L., & Rocca-Volmerange, B. 1982, A&A, 113, L15

Lequeux, J., Le Bourlot, J., Pineau des Forêts, G., Roueff, E., Boulanger, F., & Rubio, M. 1994, A&A, 292, 371

Li, A., & Draine, B.T. 2001, ApJ, 554, 778 (LD01)

Martin, N., Maurice, & Lequeux, J. 1989, A&A, 215, 219

Mathis, J.S., Mezger, P.G., & Panagia, N. 1983, A&A, 128, 212

Pauzat, F., & Ellinger, Y. 2001, MNRAS, 324, 355

Pei, Y.-C., Fall, S.M., & Bechtold, J. 1991, ApJ, 378, 6

Prévot, M.L., Lequeux, J., Prevot, L., Maurice, E., & Rocca-Volmerange, B. 1984, *A&A*, 132, 389

Reach, W.T., Boulanger, F., Contursi, A., & Lequeux, J. 2000, *A&A*, 361, 895

Rodrigues, C.V., Magalhães, A.M., Coyne, G.V., & Pirola, V. 1997, *ApJ*, 485, 618

Russell, S.C., & Dopita, M.A. 1992, *ApJ*, 384, 508

Sauvage, M., Thuan, T.X., & Vigroux, L. 1990, *A&A*, 237, 296

Schlegel, D.J., Finkbeiner, D.P., & Davis, M. 1998, *ApJ*, 500, 525

Schwering, P.B.W., & Israel, F.P. 1990, *Atlas and Catalogue of Infrared Sources in the Magellanic Clouds* (Dordrecht: Kluwer)

Stanimirovic, S., Staveley-Smith, L., van der Hulst, J.M., Bontekoe, Tj.R., Kester, D.J.M., & Jones, P.A. 2000, *MNRAS*, 315, 791

Sturm, E., Lutz, D., Tran, D., Feuchtgruber, H., Genzel, R., Kunze, D., Moorwood, A.F.M., & Thornley, M.D. 2000, *A&A*, 358, 481

Szczepanski, J., Wehlburg, C., & Vala, M. 1995, *Chem. Phys. Lett.*, 232, 221

Thompson, G.I., Nandy, K., Morgan, D.H., & Houziaux, L. 1988, *MNRAS*, 230, 429

Tielens, A.G.G.M., Allamandola, L.J., Barker, J.R., & Cohen, M. 1987, in *Polycyclic Aromatic Hydrocarbons and Astrophysics*, ed. A. Léger, L. d'Hendecourt, & N. Boccaro (Dordrecht: Reidel), 273

Tumlinson, J., Shull, J.M., Rachford, B.L., et al. 2002, *ApJ*, 566, 857

Vermeij, R., Peeters, E., Tielens, A.G.G.M., & van der Hulst, J.M. 2002, *A&A*, 382, 1042

Verstraete, L., et al. 2001, *A&A*, 372, 981

Weingartner, J.C., & Draine, B.T. 2001a, *ApJ*, 548, 296

Weingartner, J.C., & Draine, B.T. 2001b, *ApJS*, 134, 263